# Attenuation of Cutoff Modes and Leaky Modes of Dielectric Slab Structures

HERMANN A. HAUS, FELLOW, IEEE, AND DAVID A. B. MILLER, MEMBER, IEEE

*Abstract*—**A simple formula is developed for the attenuation constant of higher order cutoff modes of a dielectric slab guide and of the modes of leaky guides. The formula is based on a perturbation analysis that reduces the problem to that of the transmission characteristic of a Fabry–Perot resonator. Under certain approximations, the formula for leaky guides reduces to that of Hall and Yeh, but the formula has a wider range of applicability.**

## INTRODUCTION

WHEN a mode of a dielectric slab guide of index higher than that of the surrounding medium reaches "cutoff," it changes from a true guided mode to a radiating mode (we can also refer to these radiating modes as "leaky" or unbound). The mode's propagation constant becomes complex, indicating decay along the direction of propagation. Modes of a "capillary" guide (or leaky guide) bounded by material of index higher than that of the space occupied by the field always radiate and hence are always "leaky." Our interest in the problem of leaky modes was stimulated by the practical requirement of understanding waveguide propagation in waveguides formed from a variety of GaAs and GaAlAs layers on a GaAs substrate. In this case, the refractive index of the substrate is always at least as large as that of the layers above it. Thus, regardless of the detailed structure of those layers, there are always leaky modes of the whole structure formed by the reflection of waves in the layers off the substrate interface. This is not, of course, total internal reflection as in a true bound or guided mode, but because of the shallow angles of incidence encountered in practice, these radiating, "leaky" modes can propagate substantial distances, and will always be a potential problem in GaAlAs waveguides on GaAs substrates.

This problem became particularly acute in recent measurements of polarization dependence of absorption in quantum wells for light propagating in the plane of the thin GaAs quantum well layers [1]. The obvious way to make such a measurement is to form a waveguide containing a quantum well layer. Samples in which a conventional waveguide with low index GaAlAs "cladding" layers were formed around a "core" of higher index GaAs/GaAlAs material containing a single quantum well never showed complete absorption of the light coupled into the system, although the attenuation in the quantum well should have been sufficient. The reason was that light could propagate in the larger "leaky" mode formed due to the partial reflections from the GaAs substrate; this mode was much less strongly absorbed by the quantum well. The coupling of the incident light into the structure was never sufficiently good such that this propagation was negligible. The final solution to this measurement problem was to form only a leaky guide from the outset; the quantum well was positioned so that there was strong absorption of the first "leaky" mode, and the guide thickness was chosen so that the higher order leaky modes would be rapidly attenuated by radiation if not by absorption. This approach, with the design based partly on the model presented here, was successful both for the basic absorption [1] and also the electroabsorption [2] of the quantum well.

The key parameter in characterizing a "leaky" mode is the imaginary part of the propagation constant (i.e., the decay constant or the inverse of the $1/e$ propagation distance). One way is to solve the determinantal equation for a complex propagation constant. This has been done by Hall and Yeh [3] for the leaky slab guide. Yariv [4] derived the approximate expression of Hall and Yeh by ray-optics arguments. In this paper, we use yet another approach to arrive at the decay constant of leaky guide modes and cutoff modes. The formulas are better approximations than those previously derived, and also include the case of a dispersive medium filling the guide.

Our approach has been motivated partly by the solution methods employed in the analogous quantum mechanical problem of a particle and a rectangular potential well or barrier. The potential well has bound states analogous to guided modes of a slab guide, and also has resonant states for certain particle energies above the well which are not bound and correspond to the radiating modes of a conventional slab guide above "cutoff." The case of the potential barrier has no bound states and is analogous to the "capillary" slab guide; it also possesses resonant states above the potential barrier which are analogous to the modes of the leaky guide. Analogously, the resonant states in the quantum mechanical problem have a Fabry–Perot like character [5] since the particle (or wave) sees a reflectivity at each side of the barrier or well, and the resonant states occur when the separation between the edges of the well or barrier is an integral number of half wavelengths. The

Manuscript received March 1, 1985; revised September 23, 1985.

H. A. Haus was on sabbatical at AT&T Bell Laboratories, Holmdel, NJ 07733, when this work was performed. He is with the Department of Electrical Engineering and Computer Science, Massachusetts Institute of Technology, Cambridge, MA 02139.

D. A. B. Miller is with AT&T Bell Laboratories, Holmdel, NJ 07733.

IEEE Log Number 8406673.

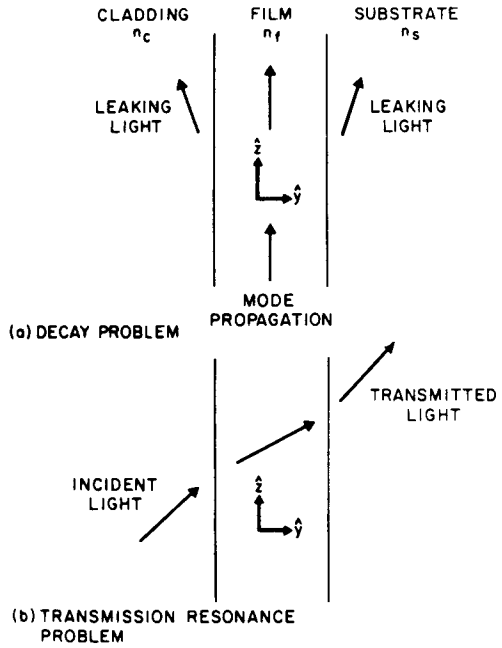


Fig. 1. The propagation directions for the waveguide "Fabry-Perot" (a) for the initial value problem or the boundary value problem (decay of internal excitation), (b) in the steady-state Fabry-Perot problem (transmission resonances under external excitation).

widths of the resonant states also give a measure of the length of time a particle spends in the resonant states before decaying out. This, therefore, suggests the use of a similar analogy in the case of the unbound modes in the waveguide problem. Now the widths of the resonances will give the decay constant of the unbound modes. A particular advantage of using the Fabry-Perot approach is that we can use the known properties of resonators to relate the decay rate of the initial excitation in the resonator to the widths of the transmission resonances. This becomes particularly simple in the case of a high-finesse resonator (the decay rate is proportional to the width), and we work within this approximation. Fig. 1 illustrates the method. In Fig. 1(a), the actual decay problem is illustrated; the light is launched in the guide and leaks out progressively into the substrate and cladding layers. In Fig. 1(b), the transmission problem is illustrated; an infinite plane wave is incident through the cladding (or the substrate) and is (partly) transmitted through the structure. The structure forms a Fabry-Perot resonator because of the reflectivities of the dielectric interfaces between the layers. The reflectivities at the interfaces are high because the wavefronts are near grazing incidence, hence satisfying the high-finesse approximation. The resonances of this structure correspond to the modes of the waveguide; for example, the lowest order mode of the waveguide will have a sinusoidal (or cosinusoidal) pattern corresponding to the internal field pattern in the lowest Fabry-Perot resonance.

In Section I, we relate the spatial decay rate of a slab mode excited in the steady state at one cross section to the temporal decay rate of the slab mode with the slabs acting as a Fabry-Perot resonator excited initially over the entire length of the slab. In this latter case, the escaping radiation accounts for the temporal decay. The temporal decay rate is in one-to-one correspondence with the width of the Fabry-Perot transmission characteristic as a function of frequency excited in the steady state. This case is most easily treated mathematically and all other mentioned phenomena can be derived through this case in the limit of high finesse. In Section II, we derive the Fabry-Perot transmission characteristic, and in Section III, we obtain the spatial decay rate. Section IV looks at some approximations that reduce our results to previously derived ones. Section V discusses the details of some field patterns of the Fabry-Perot excitation under both types of excitations—CW and initial excitation followed by decay. Finally, in the Appendix, we look at some further properties of the leaky modes.

## I. Relation Between Initial Value Problem and Boundary Value Problem

In the limit of high reflectivity at the boundary of the dielectric slab, the spatial decay of a mode of the leaky slab waveguide or the slab waveguide beyond cutoff can be related to the temporal decay rate of the mode in an initially excited Fabry-Perot resonator formed of the slab. Imagine a section of the slab excited by the mode of interest. If the wave vectors of the waves constituting the mode have a component $\beta_z$ along the $z$ axis (and $\beta_y$ along the $y$ axis), the field pattern will propagate along the $z$ axis with the group velocity $v_g = 1/(d\beta_z/d\omega)$. A temporal rate of decay given by $\mathrm{Im}(\Delta\omega)$ is transformed into a spatial rate of the decay $\alpha_z$ of the wave packet as it proceeds down the slab in the $z$ direction with the group velocity $v_g$.

$$\alpha_z = \frac{1}{v_g} \mathrm{Im}\,(\Delta\omega). \tag{1.1}$$

This argument can be put more formally in terms of a perturbation of the dispersion relation. In the absence of radiation loss, the dispersion relation is of the form

$$D(\omega, \gamma_z) = 0 \tag{1.2}$$

where $\gamma_z$ is the propagation constant in the $z$ direction. For example, with perfectly reflecting walls spaced a distance $l$ apart $D(\omega, \gamma_z) = \omega^2\mu\epsilon + \gamma_z^2 - (s\pi/l)^2 = 0$ would be the particular form of the dispersion relation for the mode of order $s$. Propagating modes have a pure imaginary $\gamma_z$, $\gamma_z = j\beta_z$. When a perturbation $p$ is introduced, (1.2) is modified to

$$D(\omega, \gamma_z, p) = 0. \tag{1.3}$$

An example of such a perturbation is the removal of the perfect reflection causing radiation loss. Differentiation of (1.2) gives

$$\frac{\partial D}{\partial \omega}\Delta\omega + \frac{\partial D}{\partial \gamma_z}\Delta\gamma_z = 0 \tag{1.4}$$

and analogously, differentiation of (1.3) gives

$$\frac{\partial D}{\partial \omega}\Delta\omega + \frac{\delta D}{\delta \gamma_z}\Delta\gamma_z + \frac{\partial D}{\partial p}\Delta p = 0. \tag{1.5}$$

The situation in which a given mode with $\gamma_z = j\beta_z$ is excited in the slab and the temporal rate of decay due to radiation is evaluated is a special case of (1.5) with $\Delta\gamma_z = 0$:

$$\Delta\omega = -\frac{\left(\frac{\partial D}{\partial p}\right)}{\left(\frac{\partial D}{\partial \omega}\right)}\Delta p. \tag{1.6}$$

This is an initial value problem.

The other form of excitation in which the slab is excited in the steady state and the spatial rate of decay is determined is another special case with $\Delta\omega = 0$, giving, according to (1.5),

$$\Delta\gamma_z = -\frac{\left(\frac{\partial D}{\partial p}\right)}{\left(\frac{\partial D}{\partial \gamma_z}\right)}\Delta p. \tag{1.7}$$

This is a boundary value problem.

Knowledge of $\Delta\omega$ from (1.6) enables one to find $\Delta\gamma_z$ from (1.7):

$$\Delta\gamma_z = \frac{\left(\frac{\partial D}{\partial \omega}\right)}{\left(\frac{\partial D}{\partial \gamma_z}\right)}\Delta\omega. \tag{1.8}$$

For small $\Delta p$, the derivatives in (1.8) are evaluated at $p = 0$, and thus (1.4) can be used to eliminate $(\partial D/\partial\omega)/(\partial D/\partial\gamma_z)$, which is

$$\frac{\left(\frac{\partial D}{\partial \omega}\right)}{\left(\frac{\partial D}{\partial \gamma_z}\right)} = -\frac{\partial\gamma_z}{\partial\omega} = -j\frac{\partial\beta_z}{\partial\omega} = -j\frac{1}{v_g} \tag{1.9}$$

where $v_g$ is the group velocity. In this way, we finally obtain (1.1) with $\Delta\gamma_z = \alpha_z$ (i.e., $\gamma_z = \alpha_z + j\beta_z$). Equation (1.1) provides a means for the evaluation of the spatial decay rate in terms of the temporal decay rate of an initially excited Fabry–Perot resonator.

The analysis of the decay of the Fabry–Perot resonator in turn can take advantage of the correspondence between the rate of decay of an initially excited mode and the transmission characteristic of the Fabry–Perot. The transmission is a steady-state problem. The energy decay rate 2 Im $\Delta\omega$ is

$$2\ \mathrm{Im}\ (\Delta\omega) = \omega_0/Q_e \tag{1.10}$$

where $Q_e$ is the external $Q$ of the resonator and $\omega_0$ is its resonance frequency. If the resonator has two escape "ports," then the decay rate is the sum of the decay rates due to the individual ports. The full width at half maximum (FWHM) of the transmission characteristic is also given by $\omega_0/Q_e$. Thus, evaluating the transmission characteristic under steady-state excitation, one finds the decay rate for the initial value problem which in turn can be related to the original (boundary value) decay problem through relation (1.1). The analysis is perturbational and thus assumes a high value of $Q_e$ ($Q_e > 10$). Fig. 1 illustrates the correspondence between the two "experiments." In the transient initial value problem, $\beta_{sy}$ and $\beta_{cy}$ (the $y$ components of Im ($\gamma$) in the substrate and cladding, respectively) point away from the slab. In the transmission problem, the incident radiation and the transmitted radiation both propagate in the positive $y$-direction. Fig. 2 lays out pictorially the correspondences among the three cases considered above.

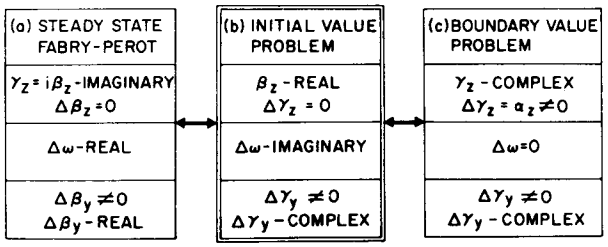


Fig. 2. Diagrams for the correspondences among the three cases: (a) steady-state Fabry–Perot (transmission resonances under external excitation), (b) initial value problem (temporal decay of a mode initially uniformly excited along the entire guide), (c) boundary value problem (spatial decay of a mode continuously excited at one end of the guide).

In the following sections, we shall analyze the decay rate of TE and TM modes beyond cutoff. We shall also develop expressions for the rate of decay in leaky slab waveguides with "substrate" and "cover" media of higher index than that of the "guiding" slab. Finally, we shall evaluate the group velocities $v_{gy}$ (the velocity of energy propagation perpendicular to the slab) and $v_{gz}$.

## II. The Transmission Fabry–Perot

The transmission "Fabry–Perot" is illustrated schematically in Fig. 3. The scattering matrices at the two surfaces are indicated. The normalized wave amplitudes on the left are denoted with subscript (1), and those on the right with subscript (2). The reflection coefficients for TE waves are (see [6, p. 58])

$$r_c = \frac{1 - \sqrt{\frac{\epsilon_c}{\epsilon_f}\frac{\cos\theta_c}{\cos\theta_f}}}{1 + \sqrt{\frac{\epsilon_c}{\epsilon_f}\frac{\cos\theta_c}{\cos\theta_f}}} = \frac{1 - \frac{n_c}{n_f}\frac{\cos\theta_c}{\cos\theta_f}}{1 + \frac{n_c}{n_f}\frac{\cos\theta_c}{\cos\theta_f}} \tag{2.1}$$

and a corresponding expression for $r_s$

$$r_s = \frac{\sqrt{\frac{\epsilon_f}{\epsilon_s}\frac{\cos\theta_f}{\cos\theta_s}} - 1}{\sqrt{\frac{\epsilon_f}{\epsilon_s}\frac{\cos\theta_f}{\cos\theta_s}} + 1} = \frac{\frac{n_f}{n_s}\frac{\cos\theta_f}{\cos\theta_s} - 1}{\frac{n_f}{n_s}\frac{\cos\theta_f}{\cos\theta_s} + 1}. \tag{2.2}$$

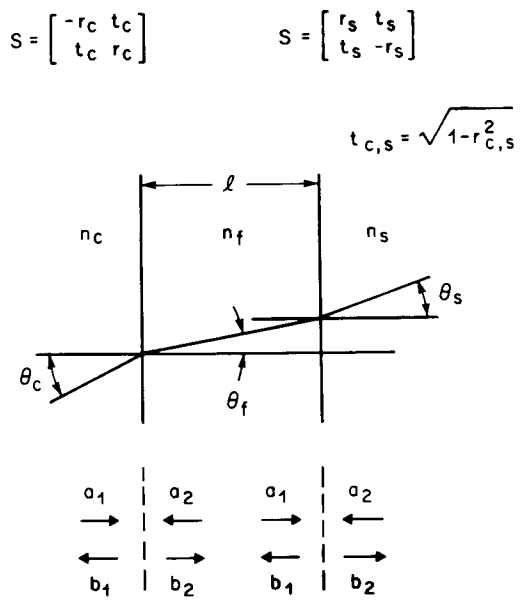


Fig. 3. Definitions of terms for dielectric slab structure.

For TM waves, the corresponding relations are

$$r_c = \frac{1 - \sqrt{\frac{\epsilon_c}{\epsilon_f}}\frac{\cos\theta_f}{\cos\theta_c}}{1 + \sqrt{\frac{\epsilon_c}{\epsilon_f}}\frac{\cos\theta_f}{\cos\theta_c}} = \frac{1 - \frac{n_c}{n_f}\frac{\cos\theta_f}{\cos\theta_c}}{1 + \frac{n_c}{n_f}\frac{\cos\theta_f}{\cos\theta_c}} \tag{2.3}$$

$$r_s = \frac{\sqrt{\frac{\epsilon_f}{\epsilon_s}}\frac{\cos\theta_s}{\cos\theta_f} - 1}{\sqrt{\frac{\epsilon_f}{\epsilon_s}}\frac{\cos\theta_s}{\cos\theta_f} + 1} = \frac{\frac{n_f}{n_s}\frac{\cos\theta_s}{\cos\theta_f} - 1}{\frac{n_f}{n_s}\frac{\cos\theta_s}{\cos\theta_f} + 1}. \tag{2.4}$$

The transmission of the Fabry–Perot defined by $T \equiv$ output intensity ÷ input intensity is (see [6, eq. (3.49)])

$$T = \frac{t_s^2 t_c^2}{(1 - r_s r_c)^2}\frac{1}{1 + \frac{4 r_s r_c}{(1 - r_s r_c)^2}\sin^2\frac{\delta}{2}} \tag{2.5}$$

where

$$\delta = 2\frac{\omega}{c} n_f l \cos\theta_f. \tag{2.6}$$

The FWHM of the transmission gives the inverse external $Q$ of the Fabry–Perot resonator according to (1.6) (Compare [6, eq. (7.54)]). From (2.5), we find the deviation of $\delta$, $\Delta\delta$ at which $T$ is reduced to half its maximum value:

$$\Delta\delta = \frac{1 - r_s r_c}{\sqrt{r_s r_c}}. \tag{2.7}$$

## III. The Rate of Decay of Leaky Modes

In the preceding section, we found the widths of the transmission window $\Delta\delta$ for the Fabry–Perot. This parameter has to be related to the temporal rate of decay of an initially excited mode in the Fabry–Perot. The temporal rate of decay in turn is related to the transmission as a function of real frequency of the Fabry–Perot. In this last "thought" experiment (the steady-state Fabry–Perot), the exciting source varies its frequency, but keeps its spatial character fixed and thus keeps $\beta_z$ fixed as the frequency is swept. This means that

$$\beta_z = \frac{\omega}{c} n_f \sin\theta_f = \text{constant} \tag{3.1}$$

(i.e., $d\beta_z/d\omega = 0$). Therefore, we find a relation for $d\theta_f/d\omega$:

$$\omega_0 \cot\theta_f \frac{d\theta_f}{d\omega} = -\left|1 + \frac{\omega_0}{n_f}\frac{dn_f}{d\omega}\right|. \tag{3.2}$$

Now, the change of $\delta$, $\Delta\delta = \Delta\omega d\delta/d\omega$ is, from (2.6),

$$\Delta\delta = 2\frac{\Delta\omega}{c} n_f l \cos\theta_f \left|1 + \frac{\omega_0}{n_f}\frac{dn_f}{d\omega} - \omega_0 \tan\theta_f \frac{d\theta_f}{d\omega}\right|. \tag{3.3}$$

Using (3.2), we find

$$\Delta\delta = 2\frac{\Delta\omega}{c} n_f l \cos\theta_f \left|1 + \frac{\omega_0}{n_f}\frac{dn_f}{d\omega}\right| \left|1 + \tan^2\theta_f\right|. \tag{3.4}$$

Solving for $\Delta\omega$ using (2.7) and (3.4), we find the inverse external $Q$:

$$\frac{1}{Q_e} = \frac{2\Delta\omega}{\omega_0} = \frac{1}{\frac{\omega_0}{c} n_f l \cos\theta_f} \cdot \frac{1}{1 + \frac{\omega_0}{n_f}\frac{dn_f}{d\omega}} \frac{1}{1 + \tan^2\theta_f} \frac{1 - r_s r_c}{\sqrt{r_s r_c}}. \tag{3.5}$$

Next, we have to convert $\Delta\omega/\omega_0$ into a spatial rate of decay using (1.1) and (1.10) (i.e., we have to convert the steady-state result to the boundary value result). The inverse group velocity is the derivative of the propagation constant with respect to frequency of $\beta_z$:

$$\frac{1}{v_{gz}} = \frac{d\beta_z}{d\omega} = \frac{d}{d\omega}\left(\frac{\omega}{c} n_f \sin\theta_f\right) = \frac{n_f}{c}\sin\theta_f \left|1 + \frac{\omega_0}{n_f}\frac{dn_f}{d\omega} + \omega_0 \cot\theta_f \frac{d\theta_f}{d\omega}\right| \tag{3.6}$$

where the mode pattern in the $y$ direction has to be kept constant.

$$\beta_{yf} = \frac{\omega}{c} n_f \cos\theta_f = s\pi = \text{constant} \tag{3.7}$$

with $s$ equal to the mode number, $s = 1, 2, 3, \cdots$, i.e., $d\beta_{yf}/d\omega = 0$. Differentiating (3.7), we obtain

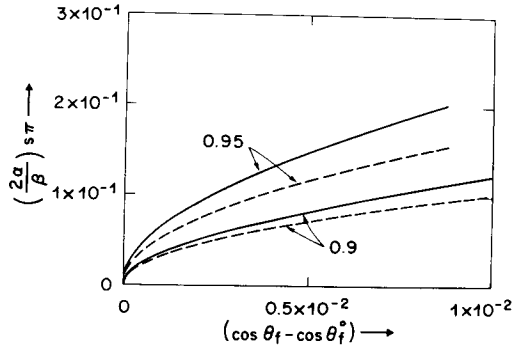


Fig. 4. Plot of $(2\alpha/\beta)\ s\pi$ versus $(\cos\theta_f - \cos\theta_f^0)$ where $\theta_f^0$ is $\theta_f$ at cutoff; TE cutoff mode for $n_c/n_f = n_s/n_f = 0.9, 0.95$.

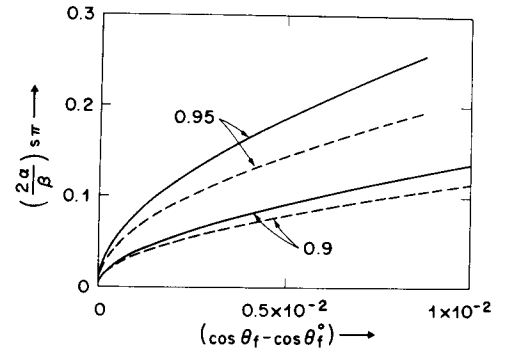


Fig. 5. Plot of $(2\alpha/\beta)\ s\pi$ versus $(\cos\theta_f - \cos\theta_f^0)$ where $\theta_f^0$ is $\theta_f$ at cutoff; TM cutoff mode for $n_c/n_f = n_s/n_f = 0.9, 0.95$.

$$\frac{\omega}{c} n_f \cos\theta_f \left[1 + \frac{\omega_0}{n_f}\frac{dn_f}{d\omega} - \omega_0 \tan\theta_f \frac{d\theta_f}{d\omega}\right] = 0. \quad (3.8)$$

Therefore, combining (3.6) and (3.8),

$$\frac{1}{v_{gz}} = \frac{n_f}{c}\sin\theta_f \left[1 + \frac{\omega_0}{n_f}\frac{dn_f}{d\omega}\right]\left[1 + \cot^2\theta_f\right]. \quad (3.9)$$

In a dispersion-free medium, $dn_f/d\omega = 0$, the above reduces to $1/v_{gz} = n_f/(c \sin\theta_f)$, which is the expression for the group velocity of a waveguide with perfectly reflecting walls. We find for the decay constant, combining (1.1), (1.10), (3.5), and (3.9),

$$2\alpha = \frac{\tan\theta_f}{l}\frac{1 - r_s r_c}{\sqrt{r_s r_c}}\frac{1 + \cot^2\theta_f}{1 + \tan^2\theta_f}. \quad (3.10)$$

This formula reduces to

$$2\alpha = \frac{\cot\theta_f}{l}\frac{1 - r_s r_c}{\sqrt{r_s r_c}}. \quad (3.11)$$

This is the desired formula. Note that the decay constant is independent of the dispersion $dn_f/d\omega$. $\theta_f$ is fixed by the mode pattern. With $s$ equal to the number of half wavelengths along the $y$ direction,

$$\theta_f = \cos^{-1}\left[\frac{s\lambda}{2n_f l}\right], \quad (3.12)$$

all other parameters in expression (3.11) are functions of $n_s/n_f$, $n_c/n_f$, and $\theta_f$. The solid curves in Figs. 4–7 (for equal

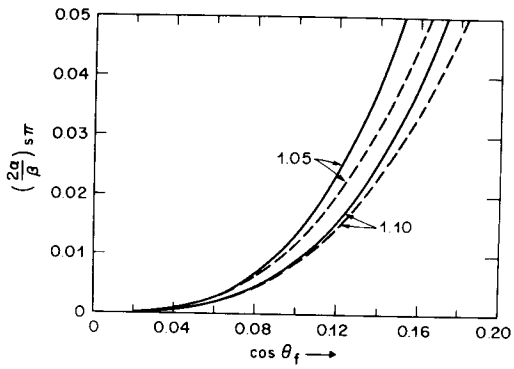


Fig. 6. Plot of $(2\alpha/\beta)\ s\pi$ versus $\cos\theta_f$; TE leaky mode for $n_c/n_f = n_s/n_f = 1.05, 1.10$.

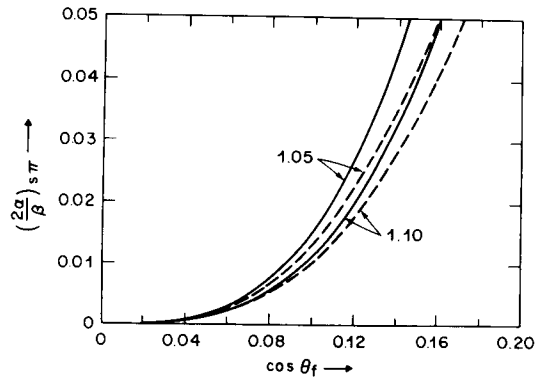


Fig. 7. Plot of $(2\alpha/\beta)\ s\pi$ versus $\cos\theta_f$; TM leaky mode for $n_c/n_f = n_s/n_f = 1.05, 1.10$.

$n_s$ and $n_c$) show the normalized attenuation $2\alpha/\beta$ for the leaky modes. Note that $\cos\theta_f = s\pi/(\omega/c)\ n_f = (s/2n_f)\ \lambda$ and thus is proportional to wavelength. The abscissas of the plots are thus proportional to wavelength. In Figs. 4 and 5, the abscissas are measured from the cutoff wavelength. Also indicated in the figures are the approximate values obtained after certain approximations that lead to the expressions of Hall and Yeh [3] and Yariv[4]. Next we turn to the approximations.

## IV. Approximate Expressions for the Attenuation Constants

If $r_s$ and $r_c$ are close to unity and $\cos\theta_f \ll 1$, we may write, instead of (3.11),

$$2\alpha \cong \frac{\cos\theta_f}{l}(1 - r_s r_c). \quad (4.1)$$

In the case of cutoff modes, the angles $\theta_s$ and $\theta_c$ are closer to $\pi/2$ than $\theta_f$. One may set

$$\cos\theta_s/\cos\theta_f \ll 1 \qquad \cos\theta_c/\cos\theta_f \ll 1$$

and write for $r_c$ and $r_s$, using (2.1) and (2.2) for TE waves,

$$r_c \simeq 1 - 2\frac{n_c}{n_f}\frac{\cos\theta_c}{\cos\theta_f}$$

$$= 1 - 2\frac{n_c}{n_f}\cos\theta_c \Big/ \sqrt{1 - \left(\frac{n_c}{n_f}\right)^2} \quad (4.2)$$

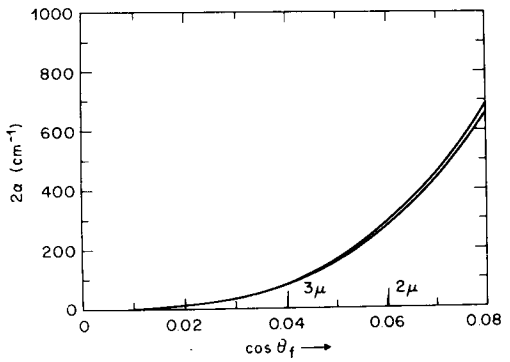


Fig. 8. Plot of $2\alpha$ [$cm^{-1}$] versus $\cos\theta_f$ for $n_s = n_c = 3.63$, $n_f = 3.515$, $\lambda = 0.85\mu$, $s = 1$; TE mode.

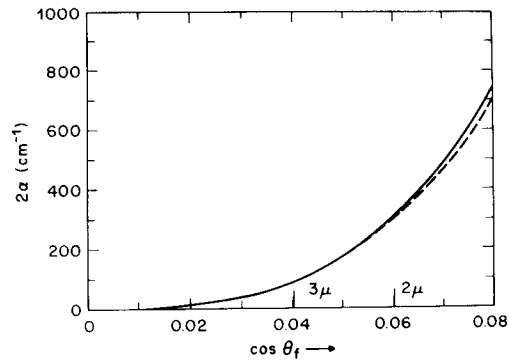


Fig. 9. Plot of $2\alpha$ [$cm^{-1}$] versus $\cos\theta_f$ for $n_s = n_c = 3.63$, $n_f = 3.515$, $\lambda = 0.85\mu$, $s = 1$; TM mode.

and a corresponding expression for $r_s$. For TM waves, one has

$$|r_c| \simeq \left(1 - 2\frac{n_f}{n_c}\frac{\cos\theta_c}{\cos\theta_f}\right)$$

$$\simeq 1 - 2\frac{n_f}{n_c}\cos\theta_c\Big/\sqrt{1 - \left(\frac{n_c}{n_f}\right)^2} \tag{4.3}$$

and an analogous expression for $|r_s|$.

In the case of the leaky guide, $\cos\theta_f$ approaches zero faster than $\cos\theta_s$ or $\cos\theta_f$. Therefore, $\cos\theta_f/\cos\theta_c \ll 1$ and $\cos\theta_f/\cos\theta_s \ll 1$, and one obtains for $r_c$, for TE waves,

$$r_c \simeq -\left(1 - 2\frac{n_f}{n_c}\frac{\cos\theta_f}{\cos\theta_c}\right)$$

$$\simeq -\left(1 - 2\frac{n_f}{n_c}\frac{\cos\theta_f}{\sqrt{1 - \left(\frac{n_f}{n_c}\right)^2}}\right) \tag{4.4}$$

and an analogous expression for $r_s$. Figs. 4–7 show the comparison between the two sets of expressions. For $\cos\theta_s \to 0$ or $\cos\theta_f \to 0$, the approximate expressions approach the more exact ones, but appreciable deviations occur even for very small attenuations per wavelength. Figs. 8 and 9 show the attenuation constant computed for a typical GaAlAs leaky guide structure with $n_c = n_s = 3.63$ and $n_f = 3.515$ at a wavelength of $\lambda = 0.85\mu$. Thickness $l$ of the film for the lowest order mode are indicated on the abscissa calibrated in terms of $\cos\theta_f = s\lambda/(2n_f l)$. Equations (4.6) and (4.8) of Table I agree with those of Hall and Yeh [3].

TABLE I
THE POWER-ATTENUATION RATE $2\alpha$

TE

Cutoff Mode
$$\frac{2}{l}\left\{\frac{n_s}{n_f}\cos\theta_s + \frac{n_c}{n_f}\cos\theta_c\right\} \tag{4.5}$$

If $\theta_s$ or $\theta_c$ is imaginary, the corresponding term is to be omitted.

Leaky Mode
$$\frac{s^2\lambda^2}{2l^3n_f^2}\left[\frac{n_f}{n_s}\frac{1}{\sqrt{1 - \left(\frac{n_f}{n_s}\right)^2}} + \frac{n_f}{n_c}\frac{1}{\sqrt{1 - \left(\frac{n_f}{n_c}\right)^2}}\right] \tag{4.6}$$

TM

Cutoff Mode
$$\frac{2}{l}\left\{\frac{n_f}{n_s}\cos\theta_s + \frac{n_c}{n_f}\cos\theta_c\right\} \tag{4.7}$$

If $\theta_s$ or $\theta_c$ is imaginary, the corresponding term is to be omitted.

Leaky Mode
$$\frac{s^2\lambda^2}{2l^3n_f^2}\left[\frac{n_s}{n_f}\frac{1}{\sqrt{1 - \left(\frac{n_f}{n_s}\right)^2}} + \frac{n_c}{n_f}\frac{1}{\sqrt{1 - \left(\frac{n_f}{n_c}\right)^2}}\right] \tag{4.8}$$

## V. The Mode Patterns of the Fabry-Perot

It is of interest to compare the mode patterns of the slab modes beyond cutoff and those of the leaky guides because they are quite different. A slab guide is surrounded by lower index material. The effective wavelength associated with propagation in the $y$ direction is shorter outside than that inside. The reflection at the wall approaches that of an open circuit. These statements enable one to draw the field patterns for the TE mode of the Fabry–Perot at different instants of time. Remember that $E_x$ and $\partial E_x/\partial y$ must be continuous at the boundary. The slab is an integer multiple of half wavelengths thick at resonance. We see from Fig. 10 that the field pattern obeys all these conditions at several instants of time. As time proceeds, the node of the external field proceeds until it coincides with the slab wall. The mode is predominantly antisymmetric with respect to the slab center, except, of course, when the node of the external field lies on the slab wall. Then it is symmetric.

The surprising feature of the plot of Fig. 10 is that the energy storage per unit length outside is very comparable to that inside. Yet the system has high $Q$. This follows from the fact that the transverse group velocity in the external region is small; the power density is small compared to $\omega_0$ times the energy per unit area of the slab. The mode is, mostly, the antisymmetric mode with $\partial E_x/\partial y \simeq 0$ at the slab boundary, which is equivalent to open-circuit boundary conditions.

A different situation prevails in leaky guides. Now the effective wavelength along $y$ is smaller outside than inside, and for the same slab thickness and for the mode of the same frequency, the field pattern evolution looks as shown

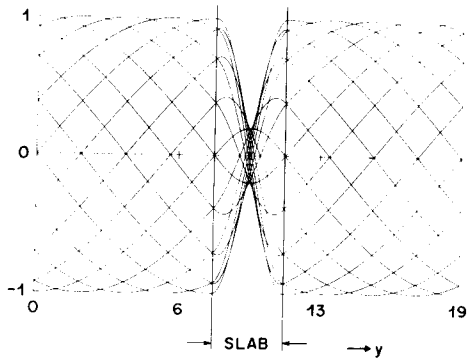


Fig. 10. Field patterns $E_y$ at resonance in transmission through the slab (for various instants in time separated by $\pi/8\omega$); TE mode (cutoff mode); $s = 1$, $n_s = n_c$, $n_f/n_s = 1.2$, $\beta_f/\beta_s = 5$.

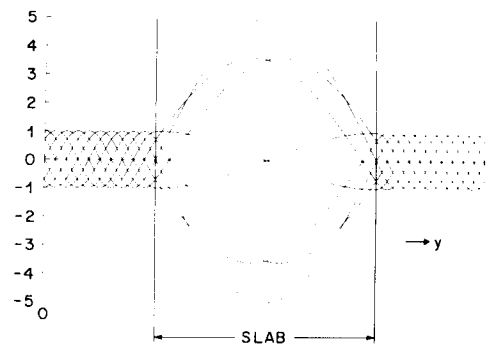


Fig. 11 Field patterns $E_y$ at resonance in transmission through the slab (for various instants in time separated by $\pi/8\omega$); TE mode (leaky guide); $s = 1$, $n_s = n_c$, $n_s/n_f = 1.2$, $\beta_s/\beta_f = 5$.

in Fig. 11. The $E$ field reaches maximum amplitude inside the slab when the node of the wave coincides with the slab wall. The pattern is predominantly symmetric with respect to the slab midplane. It is antisymmetric when the maximum of the external field amplitude occurs at the slab wall. The boundary condition of the mode is approximately that of a short circuit.

Another way to understand the boundary conditions obeyed by the leaky modes and slab modes beyond cutoff is to consider the phase change at reflection at a dielectric boundary. In the case of the leaky modes, the wave within the film sees a 180° phase shift on reflection at the interfaces to the higher index layers; this tends to cancel the incident wave, giving approximately a node at the edges of the film. In the case of the slab modes beyond cutoff, the wave within the film sees no phase change on reflection at the interfaces to the lower index material, and hence tends to have antinodes at these interfaces.

The mode patterns for the initial excitation of the Fabry–Perot (the initial value problem) and subsequent escape of radiation resemble those of Figs. 10 and 11, with some changes, of course. We can approximately evaluate the mode patterns for initial excitation of the Fabry–Perot, and compare these to Figs. 10 and 11. Our results are shown in Figs. 12 and 13. In evaluating Figs. 12 and 13, we started with the given mode pattern identified by $n_f \cos \theta_f$ from the formula $(\omega/c)n_f l \cos \theta_f = s$. Then the frequency was perturbed by Im $(\Delta\omega)$, which was evaluated

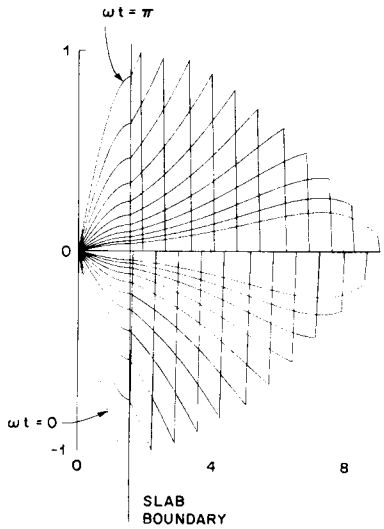


Fig. 12. Field pattern $E_y$ for initial excitation and subsequent decay; TE mode (cutoff mode); $s = 1$, $n_f/n_s = 1.2$, $\beta_f/\beta_s = 5$, $Q = 10$.

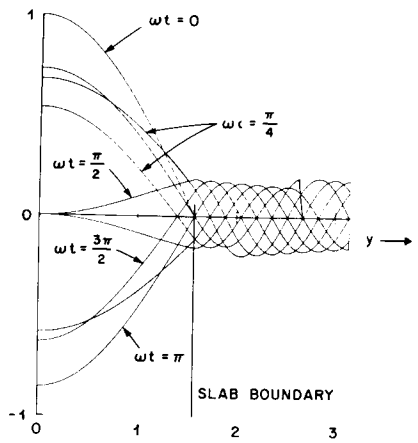


Fig. 13. Field pattern $E_y$ for initial excitation and subsequent decay; TE mode (leaky guide); $s = 1$, $n_s/n_f = 1.2$, $\beta_s/\beta_f = 5$, $Q = 10$.

from the perturbation analysis at constant $\beta_z$, producing (imaginary) changes of $\beta_{yf}$, $\beta_{yc}$, and $\beta_{ys}$. These were then used to plot the space–time evolution of the $E$ field. The mode pattern of Fig. 12 stays symmetric for all time; that of Fig. 13 remains antisymmetric. Instead of the waves moving from left to right on both sides of the Fabry–Perot, the waves now escape on the two sides in opposite directions. The slopes are not continuous, as seen in Fig. 12. This is the consequence of the perturbation approximation, which gives frequency changes correctly to first order in $1/Q$, but not the field patterns, which contain errors of order $1/Q$. Further, note the growth of the field amplitude with distance from the slab. This growth is discussed further in the Appendix.

## Conclusions

We have used the formula for the transmission characteristic of a Fabry–Perot resonator to arrive at the attenuation constant of cutoff modes and leaky modes of dielectric slab structures. The formulas for Fabry–Perot resonators derived for high $Q$ remain reliable for $Q$'s as low

as 10. One would expect, therefore, that the attenuation coefficients derived here would apply to all structures of practical interest. Appreciable deviations have been found from other approximate formulas quoted in the literature at normalized attenuation rates $2\alpha/\beta$ exceeding $10^{-2}$. It is expected that the present formulas are more accurate in these regimes of larger attenuation. We have also looked at some interesting field patterns of the slab Fabry–Perot under steady-state excitation and under an excitation at an initial time.

## Appendix

## Spatial Growth of Leaky Modes

In Figs. 12 and 13, we saw spatial growth of the field in the transverse direction as it traveled away from the slabs. This growth is contained; it does not signify an infinite energy storage per unit length if the details of the excitation are taken into account.

A brief discussion for the reasons of this behavior is in order. If the "mode" is not confined to the guide and it radiates, the propagation constant along the $z$ direction must be complex, $\gamma_{zf} = \alpha_{zf} + j\beta_{zf}$. This complex propagation constant has to be matched by the external field as shown in Fig. 14. The external field in the substrate has a spatial dependence exp $-\bar{\gamma}_s \cdot \bar{r}$ with

$$\bar{\gamma}_s = \bar{\alpha}_s + j\bar{\beta}_s. \tag{A1}$$

The $z$ components of $\bar{\gamma}_s$ must equal $\alpha_{zf}$ and $\beta_{zf}$, respectively. In a uniform loss-free medium, $\bar{\alpha}_s$ must be perpendicular to $\bar{\beta}_s$, as can be verified by substitution into the wave equation. But this means that the field grows in the $\hat{y}$ direction as shown. Of course, the growth does not persist to $y = \infty$, but persists only up to a "cone" that is determined by the source position.

Imagine a section $\Delta z$ of the guide excited by the mode pattern of interest. This is analogous to the initial excitation of a Fabry–Perot resonator over a length $\Delta z$ by a particular mode of the Fabry–Perot with dependences exp $\pm j\beta_y y$ and exp $-j\beta_z z$. The internal field of the Fabry–Perot decays as power leaks out. The propagation constant in the $y$ direction is

$$\gamma_{ys} = \sqrt{\beta_s^2 - \omega^2\mu\epsilon_s} \tag{A2}$$

and is imaginary for real $\omega$. A complex $\delta\omega$ with Im $(\delta\omega) > 0$ gives

$$\begin{aligned} \text{Re } \delta\gamma_{ys} &= \text{Re}\left[\frac{d\gamma_{ys}}{d\omega}\,\delta\omega\right] \\ &= \text{Im}\left(\frac{d\beta_{ys}}{d\omega}\,\delta\omega\right) = \frac{1}{v_{gy}}\,\text{Im}\,(\delta\omega) > 0 \end{aligned} \tag{A3}$$

where $v_{gy}$ is the group velocity in the $y$ direction of the escaping radiation.

$$\frac{1}{v_{gy}} = \frac{d\beta_y}{d\omega} = \frac{1}{c}\,n_s \cos\theta_s\left[1 + \omega_0\frac{dn_s}{d\omega} - \omega_c \tan\theta_s\frac{d\theta_s}{d\omega}\right]. \tag{A4}$$

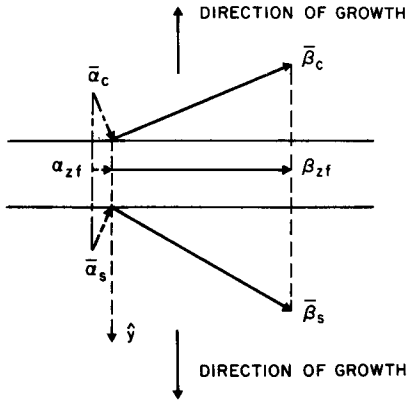


Fig. 14. The propagation vectors inside and outside the dielectric film ($f$).

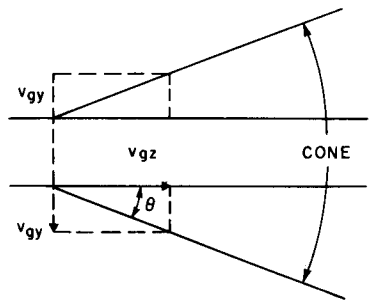


Fig. 15. The growth cone of the escaping radiation.

This group velocity measures speeds of propagation toward, and out of, the externally excited Fabry–Perot resonator. In this context, it refers to an excitation of fixed $\beta_z$, i.e., fixed $n_f \sin\theta_f = n_s \sin\theta_s$. One has the constraint (3.1) which, written in terms of $n_s$ and $\theta_s$, is of the same form, with $n_f$ replaced by $n_s$ and $\theta_f$ by $\theta_s$. Using the constraint corresponding to (3.1), one obtains from (A4)

$$\frac{1}{v_{gy}} = \frac{1}{c}\,n_s \cos\theta_s\left(1 + \frac{\omega_0}{n_s}\frac{dn_s}{d\omega}\right)[1 + \tan^2\theta_s]. \tag{A5}$$

With $v_{gy} > 0$, we have a growth exp (Im $\delta\omega)/v_{gy}$ of the escaping radiation. Because the excitation proceeds along $z$ with the group velocity $v_{gz}$, an initial excitation at $z = 0$ produces an exponentially increasing excitation that extends up to a cone of angle (see Fig. 15):

$$\tan\theta = \frac{v_{gy}}{v_{gz}} = \frac{d\beta_z/d\omega}{d\beta_y/d\omega}. \tag{A6}$$

## Acknowledgment

The authors wish to thank Dr. E. A. J. Marcatili for his critical reading of the manuscript and his helpful suggestions.

## References

[1] J. S. Weiner, D. S. Chemla, D. A. B. Miller, H. A. Haus, A. C. Gossard, W. Wiegmann, and C. A. Burrus, "Highly anisotropic optical properties of single quantum well waveguides," *Appl. Phys. Lett.*, vol. 47, pp. 664–667, 1985.

[2] J. S. Weiner. D. A. B. Miller, D. S. Chemla, T. C. Damen, C. A. Burmus, T. H. Wood, A. C. Gossard, and W. Wiegmann, "Strong polarization-sensitive electro-absorption in GaAs/AlGaAs quantum well waveguides," *Appl. Phys. Lett.*, vol. 47, pp. 1148–1150, 1985.

[3] D. B. Hall and C. Yeh, "Leaky waves in heteroepitaxial films," *J. Appl. Phys.*, vol. 44, p. 2271, 1973.
[4] A. Yariv and P. Yeh, *Optical Waves in Crystals*. New York: Wiley (Wiley Series in Pure and Applied Optics), 1984, see 11.11.1.
[5] See, for example, G. Bastard, "Quantum-size effects in the continuum states of semiconductor quantum wells," *Phys. Rev.*, vol. B30, p. 3547, 1984 and references therein.
[6] H. A. Haus, *Waves and Fields in Optoelectronics*. Englewood Cliffs, NJ: Prentice-Hall, 1984.

**Hermann A. Haus** (S'50-A'55-SM'58-F'62) was born in Ljublijana, Yugoslavia, in 1925. He attended the Technische Hochschule, Graz, and the Technische Hochschule, Vienna, Austria. He received the B.Sc. degree from Union College, Schenectady, NY, in 1949, the M.S. degree from Rensselaer Polytechnic Institute, Troy, NY, in 1951, and the Sc.D. degree from the Massachusetts Institute of Technology, Cambridge, in 1954.

He joined the Faculty of Electrical Engineering at M.I.T., where he is engaged in research in electromagnetic theory and lasers. He was a Guggenheim Fellow in 1959-1960, Visiting MacKay Professor at the University of California, Berkeley, in the summer of 1968, and Visiting Professor at the Tokyo Institute of Technology, Tokyo, Japan, in January 1980. He spent one year on leave of absence as a member of the Technical Staff at Bell Laboratories in 1974-1975. In 1984 he worked three months for Bell Communications Research and three months for AT&T Bell Laboratories. He was a Visiting Professor at the Nippon Telegraph and Telephone Corporation, Musashino, and a Fulbright Scholar at the Technical University, Vienna, in 1985. He is the author or coauthor of four books and over 100 journal articles.

Dr. Haus is a member of Sigma Xi, Eta Kappa Nu, Tau Beta Pi, the American Physical Society, the National Academy of Engineering, and a Fellow of the American Academy of Arts and Sciences. He is the recipient of the 1984 Award of the IEEE Quantum Electronics and Applications Society.

**David A. B. Miller** (M'84) was born in Hamilton, U.K., in 1954. He received the B.Sc. degree in physics from the University of St. Andrews, St. Andrews, Scotland, in 1976 and the Ph.D. degree from Heriot-Watt University, Edinburgh, Scotland, in 1979.

He remained at Heriot-Watt University until 1981, latterly as a Lecturer in the Department of Physics, before moving to Bell Laboratories, Holmdel, NJ, where he is currently a member of the Technical Staff in the Department of Laser Science Research. His research interests include low-power nonlinear optical effects in semiconductors and optical bistability.